Pergamon

Int. J. Mach. Tools Manufact. Vol. 36, No. 12, pp. 1335–1345, 1996

0890–6955/96$15.00 + .00

PII: S0890–6955(96)00025-9

AN ANALYTICAL EVALUATION OF THE CUTTING FORCES IN SELF-PILOTING DRILLING USING THE MODEL OF SHEAR ZONE WITH PARALLEL BOUNDARIES. PART 2: APPLICATION

V.P. ASTAKHOV†‡ and M.O.M. OSMAN†

(*Original received* 20 *January* 1995; *in final form* 3 *Feburary* 1996)

Abstract—This paper presents the second part of a two-part series which analyses a cutting forces model for self-piloting tools (SPT). In this second part, the influences of the tool geometry and design parameters on force calculations are analysed and a method to construct a complete force model for SPTs is proposed. For the verification of the proposed model, some selected experiments with several different geometries of SPT were carried out. Comparisons show that the theoretical results are in reasonably good agreement with the experimental data. Copyright © 1996 Elsevier Science Ltd

NOMENCLATURE

a	uncut chip thickness
$a(\xi)$	uncut chip thickness variation along the cutting edge
c_v	specific heat capacity (at constant volume) of the workpiece material
D	tool diameter in Fig. 3
F_1	friction force on the tool flank
$\mathbf{F}_{zy1}$–$\mathbf{F}_{zyn}$	cutting forces acting in the zy-plane (Fig. 3)
$\mathbf{F}_{xy1}$–$\mathbf{F}_{xyn}$	cutting forces acting on the xy-plane
f_p	complex friction coefficient
F_T, F_R, F_A	tangential, radial and axial components of the cutting force
$\mathbf{M}$	cutting moment
N_1, N_2, N_3	normal forces on the principal and auxiliary flanks
n	number of cutting elements
q_F	yield shear stress along the effective length of the chip–tool interface
R_1	location coordinate (radius) in Fig. 1
R_p	supporting pad reaction
$\mathbf{R}_s$	resultant cutting force in the zy-plane (Fig. 3)
R_x, R_{zy}	sums of projections of forces acting on the tool face into the x-axis and the zy-plane, respectively
$\mathbf{r}$	position vector of cutting-force application point with respect to the axis
s	feed (mm/rev)
$\mathbf{T}$	drive torque
T, G, Q	planes in Fig. 1
t_1, t_2, t_3, t_4	width of cutting edge parts in Fig. 4
v	cutting speed
(x, y, z)	tool coordinate system in Fig. 1
(x_1, y_1, z_1)	auxiliary coordinate system in Fig. 1
w	thermal diffusiticity of the workpiece material
α_i	flank angle at the point of interest "i"
α_{1i}, θ_{1i}, β_{1i}	angles α_i, θ_i and β_i in the section plane *I–I* (Fig. 1)
α_{2i}, θ_{2i}, β_{2i}	angles α_i, θ_i and β_i in the section plane *II–II* (Fig. 1)
α_{Ni}, θ_{Ni}, β_{Ni}	angles α_i, θ_i and β_i in the section plane *N–N* (Fig. 1)
α_{3i}	flank angle at the point of interest "i" in the section plane *III–III* (Fig. 2)
γ_{Ni}	normal rake angle at the point of interest "i"
$\gamma_N(\zeta)$	variation of the normal rake angle along the cutting edge
Δ	average percentage error
ζ	chip compression ratio
θ_i	flank angle depending upon the shape of flank at the point of interest "i"
β_i	flank angle depending upon the position of the point of interest "i" relative the tool coordinate system
λ	angle of vector $\mathbf{R}_s$ with respect to the z-axis.

†Department of Mechanical Engineering, Concordia University, Montreal, Quebec, Canada H3G 1M8.
‡Author to whom all correspondence should be addressed.

ξ_i	location angle on of the point of interest "i" in the tool coordinate system (Fig. 1)
σ_{uts}	ultimate tensile strength of the workpiece material
τ	inclination angle of the cutting edge (Fig. 1)
τ_y	yield shear stress of the workpiece material
φ_p	principal cutting edge angle (Fig. 1)
Φ_i	angles between the cutting force components and the projections of the cutting edge into zy-plane (Fig. 3)
ψ_i	angular locations of the cutting edge "i" with respect to the y-axis in Fig. 3

1. INTRODUCTION

This paper is the continuation of an earlier paper (Part 1 [1]) where a model for the analytical determination of the cutting force components acting on a drill's cutting element has been considered. The objective of this paper is to demonstrate the application of the model at the level of tool design.

The cutting force determination is essential in the design of self-piloting tools (SPT) because self-piloting drilling is a combination of metal cutting and burnishing processes. The inter-influence of these processes by means of the cutting and reaction forces is one of the prime factors which affect the quality of the machined holes. A detailed force model is necessary not only to calculate the strength of the boring bar and to choose a suitable machine tool, but also to determine the position and inter-location of the cutting and supporting-burnishing elements of SPTs. The latter calculation is also used to ensure the stability in self-piloting drilling [2]. This stability is characterized by the degree of static stability whose calculations are entirely based upon a force model. Having defined the degree of static stability, the quality of the machined holes, conditions at the tool entrance into the workpiece and even the tool life may be predicted at the level of tool and process design [3, 4].

A complete force model should include the following quantities:

(1) the magnitudes of the tangential force, F_T, radial force F_R and axial force F_A applied in the tool coordinate-system's origin;
(2) the magnitude and the direction of the cutting torque.

Given such a model, the designer would be able to optimize the tools [4, 5].

2. THE GEOMETRICAL REPRESENTATION OF SPT

As shown in Part 1, the cutting edge geometry has a significant effect on the cutting force. Experimentally, several cutting edge geometries have been developed, and both the accuracy of the machined holes and tool life have been found to have increased for an "optimum" tool geometry in a practical operation. However, this optimum geometry often cannot be reproduced because of a lack of a relevant mathematical model which is able to precisely define the geometry parameters. A comprehensive analysis of the SPT geometry and its influence on the drill performance has been made by the authors earlier [6]. This analysis, however, deals with SPTs having one cutting edge. There is a significant difference between a single edge and a multi-edge SPT in terms of the geometry analyses, even though the same approach and technique are used. For multi-edge SPTs the cutting edge is formed by the individual inserts and the position of any insert does not depend on the position of the other. In contrast, for a single edge SPT, even though this edge may contain many parts with different orientations, the geometry of any part depends on the position and geometry of other parts. Therefore a partial analysis of the multi-edge SPTs geometry is necessary.

From the point of force calculations, the important features of a cutting element of SPT are described by the variation of cutting speed, rake and flank angles along the element's cutting edge [6]. The cutting element is a three-dimensional body and its basic geometry can be analysed in the right-hand tool coordinate system (x, y, z) (Fig. 1) using the method of vector analysis. The force-related results of this analysis are set out in the following.

The normal rake angle is calculated as follows:

$$\gamma_N(\xi) = \gamma_{Ni} = \arctan(-\tan(\tau-\xi_i)\tan\varphi_p\cos\varphi_p = -\tan(\tau-\xi_1)\sin\varphi_p) \quad (1)$$

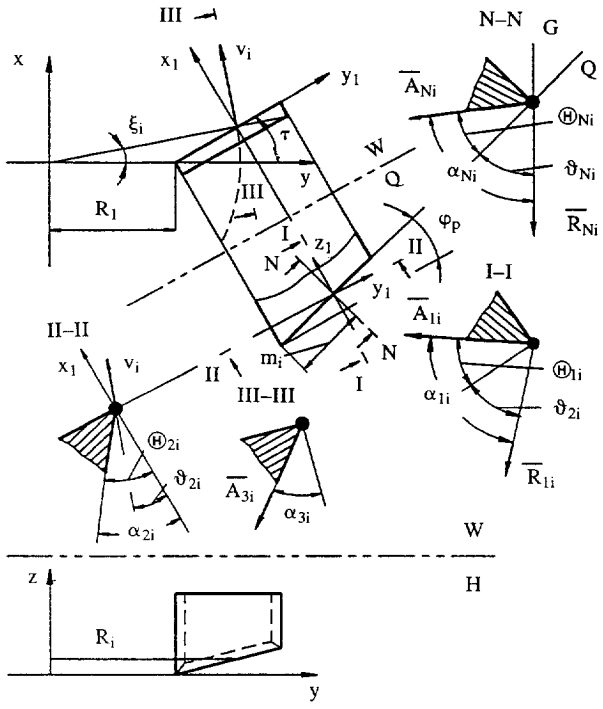

Fig. 1. Determination of rake and flank angles.

The chip thickness variation along the cutting edge can be determined as

$$a(\xi) = \frac{S}{\sqrt{1 + \left(\dfrac{\tan\varphi_p}{\cos(\tau - \xi_i)}\right)}} \tag{2}$$

The flank angle α_i at the point of interest "i" of the cutting edge can be represented by the sum of two angles (Fig. 1):

$$\alpha_i = \theta_i + \vartheta_i \tag{3}$$

where θ_i is the flank angle depending upon the shape of the flank (the flank angle is considered in the cutting element the coordinate system (x_1, y_1, z_1) [1]); ϑ is the flank angle depending upon the position of the point of interest relative to the tool coordinate system (x, y, z).

By definition, the normal flank angle α_i is the angle between plane T, which is tangent to the flank, and plane G, which is tangent to the bottom of the hole being drilled at the point of interest "i". Plane Q, which divides angle α_i into the two angles θ_i and ϑ, is perpendicular to the yz-plane. Therefore angle ϑ is the angle between the planes G and Q while angle θ_i is the angle between planes T and Q. Figure 1 shows the following angles:

- θ_{1i}, ϑ_{1i} and α_{1i} are the angles in the section plane *I–I* which is perpendicular to the y-axis and passes through the point of interest "i";
- θ_{2i}, ϑ_{2i} and α_{2i} are the angles in the section plane *II–II* which is perpendicular to the section plane *I–I* and passes through the point of interest "i";
- θ_{Ni}, ϑ_{Ni} and α_{Ni} are the angles in the section plane *N–N* which is perpendicular to the cutting edge at the point of interest "i".

The flank angles can also be defined in the section plane *III–III* which passes through the point of interest "i" and is tangent to the cylinder with a radius of R_i (Fig. 1). These

flank angles become very important in the design of trepanning SPT when the revolved view of cutters (cutting elements) is considered.

The basic relationship for the flank angles are as follows:

$$\tan\theta_{Ni} = \tan\theta_{1i}\cos\varphi_p \tag{4}$$

$$\tan\theta_{1i} = \tan\theta_{2i}\tan\varphi_p \tag{5}$$

It can be seen from Fig. 1 that $\vartheta_{2i}=\xi_i$, and thus

$$\tan\vartheta_{Ni} = \tan\vartheta_{1i}\cos\varphi_p \tag{6}$$

$$\tan\alpha_{3i} = \tan\varphi_p\sin\vartheta_{2i} + \tan\theta_{1i}\cos\vartheta_{2i}$$

$$\tan\theta_{Ni} = \tan\alpha_{2i}\frac{\cos\varphi_p}{\tan^{-1}\vartheta_{2i}} - \tan\vartheta_{2i}\sin\varphi_p \tag{7}$$

It is worth noting here that:

- The rake angles vary continuously along the cutting edge and depend upon the design parameters of the tool such as the angles φ_p, τ and radius R_1. By choosing the rake surface location it is possible to achieve any desirable distribution of rake angles along the cutting edge. Therefore the force distribution along the cutting edge is a matter not only of the cutting regime and the involved material properties, but also of the tool design. As follows from Equation (1), any meaningful force distribution along the cutting edge can be achieved by a proper choice of SPT geometry.
- The flank angles vary continuously along the cutting edge and depend upon the ground flank angles and the position of a cutting element relative to the tool coordinate system. By carefully choosing the position of the flank plane, it is possible to achieve any desirable distribution for the flank angles along the cutting edge.

3. CUTTING FORCE MODEL

A complete force model includes a number of sub-models for the force components acting on each cutting insert. Similar to the cutting edge which is the geometrical "sum" of all individual inserts in the cutting, the complete force model is the vectorial sum of the force components acting on these inserts. Therefore the model consideration includes two successive stages. The first stage includes the determination of the force components acting on each insert in the coordinate system (x_1, y_1, z_1) which is the machine reference-system described in Part 1 [1]. The second stage deals with the inserts arrangement [7], the calculation of the total force components in the tool coordinate system (x, y, z), and, as the final step, the design optimization [4].

3.1. *Force components in the coordinate system* (x_1, y_1, z_1)

The cutting force components acting on each individual insert are determined using Eqns (23–25) of Part 1 [1]. Since in a general case of the cutting insert location the geometry parameters and chip thickness vary along the insert's cutting edge, the calculation of the force components should account for these variations. Specifically, the combination of Eqns (19–21) from Part 1 [1] with functions $a(\xi)$ and $\gamma(\xi)$ defining the variations [Equations (1) and (2)] gives

$$\frac{q_F}{\sigma_{uts}} = \int_0^{\xi_{max}} \frac{\tau_y}{\sigma_{uts}}\left(1-39{\cdot}10^{-3}\left(\frac{\tau_y}{\sigma_{uts}}\frac{\sigma_{uts}}{100\,c_v}\right)^{0.8}\left(\frac{va(\xi)}{w}\frac{l_p}{a(\xi)}\frac{1}{\zeta}\right)^{0.4}\right)d\xi \tag{8}$$

where

$$\frac{\tau_y}{\sigma_{uts}} = \frac{1}{1 + 0.5 \cdot 10^{-3} \frac{\sigma_{uts}}{c_v} \frac{\zeta + \frac{1}{\zeta} - 2\sin[\gamma(\xi)]}{\cos[\gamma(\xi)]}} \tag{9}$$

To calculate the force components on the insert's flanks (N_1–N_3 and F_1), Eqn (36) from Part 1 [1] can be used.

To predict the cutting force components using the proposed approach, the chip compression ratio ζ has to be defined. Its value can be either calculated analytically using the results of Part 1 or defined experimentally. In the latter case the use of a special method for the experimental determination of the chip compression ratio in machining with SPT [8] is essential to reduce the time and increase the accuracy of the experiments.

It is known that the chip compression ratio ζ depends upon the cutting parameters [9]. Among them the cutting speed and feed are of prime importance [10]. Therefore, for each particular combination of the cutting speed and feed, the chip compression ratio should be defined separately. A typical result of the experimental determination of ζ for SPTs is given in Fig. 2(a) (outer cutting edge of the indexable cutting insert, workpiece material AISI 1040; 220 *HB*; tool material carbide C-60; tool geometry ISO 3001/1 (1977); the cutting edge angle 18°; the rake angle 0°; the inclination angle 3°; method of the determination of ζ as suggested in [8]). Difficulties arise when one tries to define the chip compression ratio for each particular combination of the cutting speed and feed. This can be avoided by plotting ζ against the product "*va*". Figure 2(b) shows that the experimental points which correspond to different feeds can be approximated by a single curve. Therefore only two tests need to be carried out to define the chip compression ratio within the experimental range. Table 1 shows the plan and results [taken from Fig. 2(b)] of the experiments. The approximation equation for the chip compression ratio is

$$\zeta = \zeta_0 \left(\frac{va}{\sqrt{(va)_1 (va)_2}} \right)^x \tag{10}$$

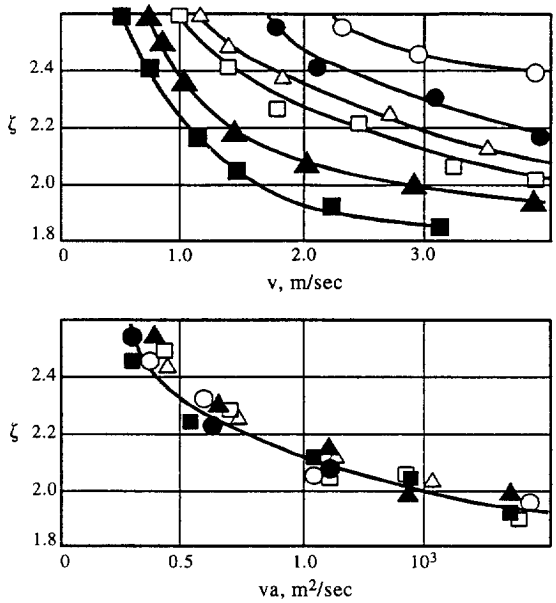

Fig. 2. Relationships between the chip compression ratio ζ, cutting speed v and product va for different feeds: ○, S=0.125 mm/rev; ●, S=0.195 mm/rev; △, S=0.285 mm/rev; □, S=0.390 mm/rev; ▲, S=0.490 mm/rev; ■, S=0.780 mm/rev.

Table 1. Plan and results of tests

Experiment number	$10^3 va$ (m²/s)	ζ
1	0.25	2.6
2	1.85	1.93

where

$$\zeta_0 = \sqrt{\zeta_1 \zeta_2} \tag{11}$$

and

$$x = \frac{\ln(\zeta_2/\zeta_1)}{\ln[(va)_1 (va)_2]} \tag{12}$$

The substitution of the experimental results from Table 1 to Equations (10)–(12) gives

$$\zeta = 2.24\left(\frac{va}{0.68 \cdot 10^{-3}}\right)^{-0.15}, \quad (0.25 \cdot 10^{-3} \leq va \leq 2 \cdot 10^{-3} \text{ (m}^2\text{/s)}) \tag{13}$$

Since the experimental determination of the chip compression ratio is relatively simple and does not require any special measuring equipment, it can be done even in machine-shop conditions.

3.2. *Total force and torque of SPT (in the tool coordinate system)*

Having defined the cutting force components acting on all SPT's inserts, the total trust and torque of SPT are determined by vectorially summing these components. At this point, a design model for SPT should be considered [2-5].

To better visualize this procedure, the model of an unsymmetrical multi-edge SPT is presented in Fig. 3. The problem of cutting force determination is described in the tool

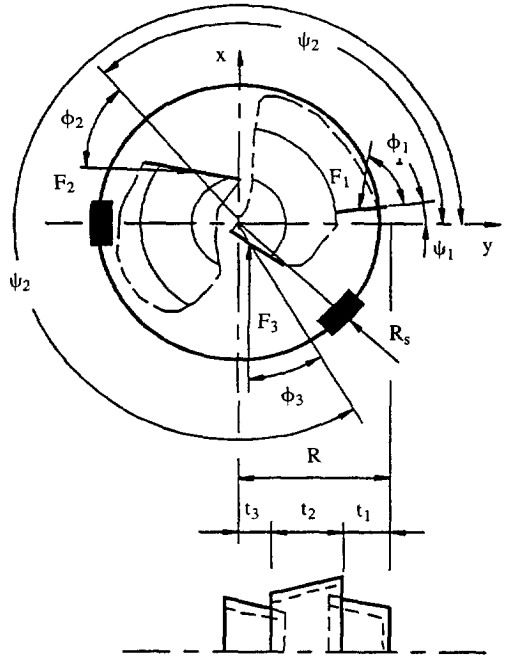

Fig. 3. Solid boring SPT with three staggered cutters.

coordinate system for a SPT of n cutting edges. The tool coordinate system, illustrated in Fig. 3, is described as:

- the x-axis is the SPT axis with positive direction toward the SPT shank;
- the y-axis is perpendicular to the x-axis and goes through the SPT corner (SPT's periphery point);
- the z-axis is perpendicular to the x- and y-axes.

Now, if $\mathbf{F}_{zy1}$, $\mathbf{F}_{zy2}$,..., $\mathbf{F}_{zyn}$ are the cutting force forces acting on zy-plane, $\mathbf{M}$ is the cutting moment and $\mathbf{R}_s$ is the force resultant in zy-plane, then from the equilibrium conditions it follows that [2–5, 7, 11]

$$\mathbf{M} = -\sum_{i=1}^{n} (\mathbf{r}_i \times \mathbf{F}_{zyi}) \tag{14}$$

and

$$\mathbf{R}_s = \sum_{i=1}^{n} \mathbf{F}_{zyi} \tag{15}$$

Expressing Equation (15) in complex form, we have

$$\mathbf{R}_s = |\mathbf{R}_s| \exp(j\lambda) = \sum_{i=1}^{n} |\mathbf{F}_{zyi}| \exp j(\psi_i + \Phi_i) \tag{16}$$

where λ is the angle of vector $\mathbf{R}_s$ with respect to the y-axis.

Equation (16), written in the trigonometric form, gives the magnitude $|\mathbf{R}_s|$ and the direction angle λ of the resultant $\mathbf{R}_s$:

$$|\mathbf{R}_s| = \left[\left(\sum_{i=1}^{n} |\mathbf{F}_{zyi}| \cos(\psi_i + \Phi_i) \right)^2 + \left(\sum_{i=1}^{n} |\mathbf{F}_{zyi}| \cos(\psi_i + \Phi_i) \right)^2 \right] \tag{17}$$

$$\lambda = \operatorname{artan} \left(\frac{\sum_{i=1}^{n} |\mathbf{F}_{zyi}| \sin(\psi_i + \Phi_i)}{\sum_{i=1}^{n} |\mathbf{F}_{zyi}| \cos(\psi_i + \Phi_i)} \right) \tag{18}$$

Here angles ψ_i are the location angles of SPT cutting elements with respect to the tool coordinate system.

Having defined the initial values of the torque, the resultant and its direction, it is possible to start the tool optimization. The optimization procedure has been presented earlier [4–7] and includes the adjustment of the supporting pads relative to the cutting inserts to achieve the identical pad reactions. The analysis of the force system shows that the identical pad reactions are achieved by their unsymmetrical location relative to the direction of the resultant. By controlling the insert locations ψ_i, directions of the cutting-force components $\mathbf{F}_{zyi}$ (angles Φ_i) and number of SPT cutting inserts, n, the conditions necessary for tool guidance, static stability and stability at the entrance of the hole being drilled can be achieved [4].

Having completed the optimization procedure, the force components which are necessary for the machining process and machine tool design can be determined as follows.

The drive torque, T is defined as

$$T = M + 2f_p R_p \tag{19}$$

Here R_p is the defined supporting pad reaction and f_p is a complex friction coefficient in the pad–workpiece contact [11].

The axial force F_A is defined as

$$F_A = \mathrm{Proj}_x\left(\sum_1^n \mathbf{F}_{xyn}\right) \tag{20}$$

Here $\mathbf{F}_{xy1}$–$\mathbf{F}_{xyn}$ are the forces acting on the xy-plane.

Besides a common use of these force factors, one extremely important but often forgotten aspect is the buckling stability of the boring bar. To calculate this stability, the mutual action of the torque and the axial force must be taken into account. As a criterion of stability, the maximum deflection of the boring bar from its longitudinal axis equal to 0.04 mm is used [4]. Where it is impossible to ensure this value, stationary or moving steady rests are used to ensure the stability within the whole machining cycle. Therefore checking the buckling stability is not only important at the machine tool and tool design stage, but also at the level of the process design when choosing a drilling machine arrangement, cutting regime, fixtures, etc.

4. EXPERIMENTAL VERIFICATION OF THE RESULTS

In order to assess the accuracy of the above proposed prediction of the cutting-force components, a series of experiments were conducted with the specially designed SPT head without the supporting pads [12]. The geometry of this head is shown in Fig. 4. In order to obtain the maximum information about the components of the cutting force and the torque on different parts of the tool cutting edge, the study was conducted separately for each part, i.e. each of parts 1–4, of the cutting edge (Fig. 4). In the experiments the head was located in a special starting bushing which was a part of a force dynamometer. The dynamometer design and its static and dynamic calibrations have been presented in details earlier [13]. The method proceedure of experiments was as described in [12, 13].

The conditions of the tests were as follows:

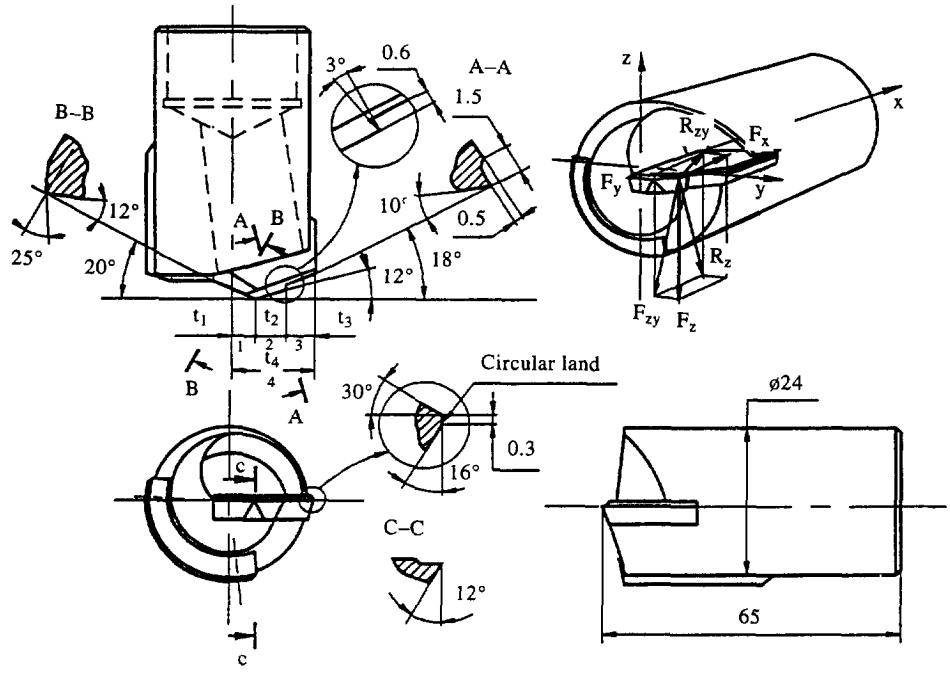

Fig. 4. Simulator of SPT used in experiments.

- Machine—a special NC deep-hole drilling machine with a high pressure cutting fluid flow station was used (Deep-Hole Machining Industrial Centre of Concordia University). The station was capable of delivering a flow of up to 220 l/min and generating a pressure of 4.5 MPa. The stationary workpiece–rotating tool working method was used in the experiments.
- Workpiece material—AISI 1040, σ_{uts}=580 MPa. The characteristics of the workpiece material are identical to those described in Part 1 except the length of the test bars which was chosen to be 700 mm in this case. The length and the shape of the working part of the workpiece were chosen in accordance with the STP diameter, keeping conditions close to the working conditions for SPTs.
- Cutting tool—specially designed SPT heads with internal chip removal 26 mm in diameter were used. The tool material was carbide C-6. The detailed diagram in Fig. 4 shows the drill's design and geometry. The cutting edge is divided into three sections: the outer and the middle cutting edges, separated by a step, are at 18 and 12°, respectively. The inner cutting edge is reversed so that an edge rather than a point is at the centre of rotation. The offset is approximately 15% of the radius. The rake angle for the inner cutting edge is −30° in comparison to 0° for the outer and middle cutting edges. The geometry parameters of drills were controlled according to standard B94.50 (1975). Tolerances for all angles were ±0.5°. The roughness R_a of the face and flank of the drills was less than 0.25 μm as measured according to standard ANSI B46.1 (1978). Each cutting edge was examined at magnification of 15× for visual defects such as chips or cracks. A special method for microcrack detection on the face and flanks was used [14].
- Cutting fluid—"Shell Garia H" cutting fluid was used in the experiments. The reservoir temperature was maintained at 27±3°. A precision turbine flow meter to measure the cutting fluid flow rate to an accuracy of ±1% was used in the experiments. Special attention was paid to chip removal [15] and to reducing the influence of the tool head design on the hydrodynamic processes in the machining zone [16].
- Parameters of experiments—the following parameters were selected as the cutting conditions:
  - t_1=2.7–6.5 mm;
  - t_2=1.8–6.3 mm;
  - t_3=3.0–6.3 mm;
  - t_4=D/2=13 mm=constant;
  - s=0.062–0.125 mm/rev;
  - v=40–90 m/min.
- Statistical analysis of the results—the 2^2 factorial, complete block type of design of experiments was used to establish the experimental force relationship [17]. The mathematical models obtained as regression equations have been statistically analysed. Such an analysis included the examinations of variance homogeneity, the significance of the model coefficients and the model adequateness [17].

The experimental results are shown in Table 2. The measured results are shown and compared with the theoretical prediction in Table 3. The average percentage error, Δ, is defined as

Table 2. Experimental results

Cutting edge number (Fig. 4)	Statistical relationship for the cutting force components		
	F_z (N)	F_y (N)	F_x (N)
1	$1497\ t^{0.98}\ S^{0.81}$	$450\ t^{1}\ S^{0.81}$	$594\ t^{0.94}\ S^{0.61}$
2	$1560\ t^{0.99}\ S^{0.78}$	$585\ t^{1.07}\ S^{0.96}$	$636\ t^{0.93}\ S^{0.66}$
3	$1620\ t^{0.94}\ S^{0.77}$	$770\ t^{0.92}\ S^{0.90}$	$728\ t^{0.93}\ S^{0.63}$

Table 3. Comparison of predicted and measured cutting force components for 1040 steel

S (mm/rev)	F_z (N)			F_y (N)			F_x (N)		
	Measured	Predicted	Error	Measured	Predicted	Error	Measured	Predicted	Error
				t_1=2.7 mm, t_2=4 mm, t_3=6.3 mm, t_4=D/2=13 mm=constant					
0.07	2609	2478	5	496	536	8	1729	1884	9
0.10	3439	3784	10	698	631	9.6	1938	1724	11
0.12	3966	4265	7.5	831	874	5.2	2207	2356	6.8
				t_1=4 mm, t_2=6 mm, t_3=3 mm, t_4=D/2=13 mm=constant					
0.07	2418	2265	6.3	712	775	8.8	1592	1462	8.2
0.10	3201	3612	12.8	423	369	12.8	1747	1856	6.2
0.12	1046	932	10.9	510	550	7.8	2003	1867	6.8

$$\Delta = \left(\frac{\text{Calculated value} - \text{measured value}}{\text{Measured value}}\right) \times 100 \tag{21}$$

As expected, the errors shown in Table 3 give no regular trend. It is partially explained by the complexity of SPT regrinding. In regrinding it is difficult to maintain the tool geometry within a close tolerance, even though a specially designed grinding fixture along with frequent dressing of a grinding wheel and a toolmaker's microscope were used. The prediction accuracy is actually acceptable in engineering practice.

The above comparison shows that the theoretical prediction agrees with the experimental data reasonably well, and so the cutting force components of SPT can be defined directly in any particular case using the proposed model without further cutting tests.

5. CONCLUSIONS

A method for predicting the cutting force components and torque in machining with SPTs is proposed and discussed. The important features of a cutting element (inserts) of SPT are described by the variation of its geometry and cutting speed along the cutting edge. An analysis of the SPT geometry results in the derivation of a force model in the insert coordinate system. A complete force model for SPTs was obtained by consideration of sub-models for force components acting on each cutting insert. Having established the force model, an optimization procedure which includes the adjustment of the supporting pads relative to the cutting inserts can be completed. To assess the accuracy of the proposed force prediction, a series of carefully planned and conducted experiments were carried out. The comparison of the predicted and experimental values shows reasonably good agreement.

This study provides further evidence of the value of the cutting mechanics approach for the prediction of important performance characteristics for such a geometrically complex practical machining operation as self-piloting machining.

Acknowledgements—The financial support of the Natural Science and Engineering Research Council of Canada is gratefully acknowledged. We would like also to express our sincere gratitude to the unknown reviewers of the paper for providing constructive criticism toward the final improvement of the manuscript.

REFERENCES

[1] V. P. Astakhov and M. O. M. Osman, An analytical evaluation of the cutting forces in self-piloting drilling using the model of shear zone with the parallel boundaries. Part 1: Theory, *Int. J. Mach. Tools Manufact.* **36**(11), 1187–1200 (1996).

[2] F. Pflegher, Aspecte Zur Konstructiven Gestaltung von Tiefbohrwerzeugen, *Werkstattstechnic* **67**(4), 211 (1977).

[3] F. Pflegher, The aspect of stability in designing deep hole drilling and boring tools. *2nd Int. Conf. on Deep Hole Drilling and Boring*, Brunel University, London (1979).

[4] V. P. Astakhov, V. V. Galitsky and M. O. M. Osman, An investigation of the static stability in self-piloting drilling, *Int. J. Prod. Res.* **33**(6), 1617 (1995).

[5] V. N. Latinovic, R. Blakely and M. O. M. Osman, Optimal design of multi-edge cutting tools for BTA deep hole machining, *Trans. ASME. J. Engng Ind.* **101**, 281 (1979).

[6] V. P. Astakhov, V. V. Galitsky and M. O. M. Osman, A novel approach to the design of self-piloting drills

with external chip removal. Part 1: Geometry of the cutting tip and grinding process, *Trans. ASME J. Engng Ind.* **117**, 453 (1995).
[7] V. N. Latinovic and M. O. M. Osman, Optimal design of BTA deep-hole cutting tools with staggered cutters, *Int. J. Prod. Res* **27**(1), 153 (1989).
[8] V.P. Astakhov and S.S. Fotty, Method of the experimental determination of the chip compression ratio. Patent no. 1004012 (USSR) (1983).
[9] N.N. Zorev, *Metal Cutting Mechanics*. Pergamon Press, Oxford (1966).
[10] V. P. Astakhov and M. O. M. Osman, Correlations among the process parameters in metal cutting and their use for establishing the optimum cutting speed, *J. Mater. Process. Technol.* **54**(4), 18 (1995).
[11] B. J. Griffiths, Modelling complex force systems. Part 1: The cutting and pad forces in deep drilling, *Trans. ASME. J. Engng Ind.* **115**, 169 (1993).
[12] V. P. Astakhov, A. A. Ajrikjan and G. M. Petrosjan, Pad forces in self-piloting drilling and their experimental determination, *UKRNIINTI* **1209**, 7 (1979).
[13] S. Chandrashekhar, M. O. M. Osman and T. S. Sankar, An experimental investigation for the stochastic modelling of the resultant force system in BTA deep hole machining, *Int. J. Prod. Res.* **23**, 65 (1985).
[14] V.P. Astakhov, S.L. Evtifeev, A.P. Gnafjuk and O. Raddats, Method of detecting the hidden surface defects on carbide inserts. Patent no. 1667491 (USSR) (1991).
[15] V. P. Astakhov, P. S. Subramanya and M. O. M. Osman, An investigation of the cutting fluid flow in self-piloting drills, *Int. J. Mach. Tools Manufact.* **35**(4), 547 (1995).
[16] V. P. Astakhov, P. S. Subramanya and M. O. M. Osman, Theoretical and experimental investigations of coolant flow in inlet channels of the BTA and ejector drills, *Proc. Inst. mech. Engr, Part B: J. Engng Manufact.* **209**, 211 (1995).
[17] V.P. Astakhov and N.L. Shlafman, *Mathematical Modelling of Machine Tools and Machine Tool Complexes* (in Russian). O.P. University Press, Oddessa (1992).